crystals

MDPI

Article

The Co-Crystallization of 4-Halophenylboronic Acid with Aciclovir, Caffeine, Nitrofurazone, Theophylline, and Proline in Function of Weak Interactions

Ventsislav Dyulgerov, Hristina Sbirkova-Dimitrova *, Kostadin Iliev and Boris Shivachev *

Institute of Mineralogy and Crystallography "Acad. Ivan Kostov", Bulgarian Academy of Sciences, Acad. G. Bonchev Str., bl. 107, 1113 Sofia, Bulgaria

* Correspondence: sbirkova@mail.bg (H.S.-D.); blshivachev@gmail.com (B.S.)

Abstract: Co-crystallization experiments of 4-halophenylboronic acid with several pharmaceutical compounds (including aciclovir, caffeine, nitrofurazone, and proline) produced several new molecular complexes. The experiments involved varying the solvent and the molar ratio of boronic acid to a pharmaceutical compound (e.g., 1:1, 2:1, 1:2). The screening process for new crystal phases revealed that the formation of the different molecular complexes was strongly influenced by the molar ratio and the presence or absence of water in the solvent. The new molecular crystals were characterized through single crystal X-ray diffraction and differential scanning calorimetry (DSC) analyses. The single crystal analyses of the molecular complexes revealed an unexpected variety in the hydrogen bonding network interactions that can be produced by the $-B(OH)_2$ motif.

Keywords: hydrogen-bonding interactions; single crystal; boronic acid; API; DSC

Citation: Dyulgerov, V.; Sbirkova-Dimitrova, H.; Iliev, K.; Shivachev, B. The Co-Crystallization of 4-Halophenylboronic Acid with Aciclovir, Caffeine, Nitrofurazone, Theophylline, and Proline in Function of Weak Interactions. *Crystals* **2023**, *13*, 468. https://doi.org/10.3390/cryst13030468

Academic Editors: Hidehiro Uekusa and Yuda Prasetya Nugraha

Received: 18 January 2023
Revised: 6 March 2023
Accepted: 7 March 2023
Published: 9 March 2023

1. Introduction

The predictable and repeatable establishment of weak intermolecular interactions underlies co-crystal formation and is often stated as a "pillar" in crystal engineering [1]. One usually associates those interactions with hydrogen bonding, though the contribution of different types of several other weak interactions (e.g., $\pi \ldots \pi$, $CH_3 \ldots \pi$, $CH \ldots O$ etc.) is not always accounted for. Normally the three-dimensional arrangement of the molecules in the crystal tends to produce the densest packing and to accommodate the greatest number of weak interactions, taking into account their strength, directionalities, etc. In order to obtain the densest packing, a molecule of the solvent(s) may also be incorporated, and thus crystal solvates are obtained. Using a preliminary designed scheme based on the expected appearance of a reproducible hydrogen bonding interaction (motif), one can attempt and eventually control the initial assembly of the molecules constructing the solid crystalline state. The ability to intentionally alter a specific atom or group in the molecule would allow finetuning of the crystallization process. Even minimal isostructural/isotypical variations at the molecular structure level (e.g., substitution or rearrangement, permutation of atoms, replacement of one functional group with another) often drastically changes unit cell parameters and the space group and produces entirely new crystalline phases. Crystal engineering is hampered by the appearance of unpredictable polymorphic forms that are related to the ability of a particular molecular species to exist in different crystalline arrangements [2–5]. Although the concept is simple and straightforward, i.e., identify a repeatable intermolecular bonding motif and implement it for obtaining a desired "pair up" or pattern, in practice one may find that nothing goes according to the envisaged scheme. Boron-containing compounds, and in particular boronic acids, $R–B(OH)_2$, are of interest for applications in organic synthesis (Suzuki reaction) [6,7], macromolecular chemistry [8–10], crystal engineering [11,12], and molecular recognition (sugar sensors) [13,14]. In addition, pharmaceutical chemistry shows an increasing interest for boron compounds, since some of

them have shown antitumor (Bortezomib) [15,16], antiviral [17], antifungal [18], or cytotoxic properties [19]. Organic boronic acids possess a $-B(OH)_2$ moiety that can theoretically participate in the establishment of predictable and repeatable $R_2^2(8)$ hydrogen bonding interactions [20,21]. Thus, boronic acids can be used as a building block in the preparation of molecular complexes based on the possible self-complementary interaction pattern. One should note that $-B(OH)_2$ moiety has a conformational flexibility regarding hydroxyls hydrogen atom (H atom). The $B(OH)_2$ moiety H atom orientation and positioning is formally distinguished as *syn*/*syn*, *syn*/*anti*, and *anti*/*anti* [22]. In this article, we report on co-crystallization trials of 4-chlorphenylboronic acid (4ClB) with a series of pharmaceutical drugs, namely: Theophylline (TEO), Caffeine (CAF), Nitrofurazone (NIT), Aciclovir (ACL), Diltiazem (DIL), Paracetamol (PAR), Indometacine (IND), some amino acids Proline (Pro), Serine (Ser), Phenylalanine (Phe), and Arginine (Arg). These drugs have a broad application in practice, and many of them are used in different fields of medicine. Of interest are the studies of the mentioned drugs in the treatment of cognitive impairment caused by diseases such as dementia and Alzheimer's (AD). Caffeine [23,24], Theophylline [25], Indometacine [26], Diltiazem [27], and particularly Aciclovir [28–30] are the subject of modern studies in the field of symptomatic improvement in the pathogenesis of AD patients. In addition, there are recent studies which report the improvement in the treatment of AD by the use of boron-containing compounds such as Aβ aggregation inhibitors and boronic acids which prevent drug leakage for AD combination treatments [31–34]. The co-crystals reported in the article could serve as a reliable starting point to improve existing drugs and expand their application.

2. Materials and Methods

2.1. Materials

The active pharmaceutical ingredients were purchased from Sigma Aldrich (Merck; Darmstadt, Germany), and the boronic acid was purchased from Frontier Scientific Inc. (Newark, DE, USA). All the solvents for the co-crystallization experiments were purchased from Sigma Aldrich (Merck; Darmstadt, Germany) and Alfa Aesar (Kandel, Germany) and were used without further purification. The co-crystallization experiments were performed using L-proline hydrate (P8865 Sigma Aldrich; Darmstadt, Germany), not a racemic D,L-proline mixture.

2.2. Co-Crystallization Experiments

The co-crystallization experiments were carried out with 1:1, 1:2, and 2:1 molar ratios of boronic acids vs drugs/amino acid. The compounds were carefully mixed in an agate mortar (manual grinding) and then dissolved in water, ethanol, methanol, or 1:1 v/v mixtures of water:ethanol, water:methanol, or ethanol:methanol (depending on the solubility of each compound). Crystals (co-crystals) of 4ClB:PRO (1:1), 4ClB:NIT (1:1), 4ClB:ACL (1:1), 4ClB:TEO (1:1), and 4ClB:CAF (2:1) were obtained by slow evaporation of the solutions at room temperature. No co-crystal formation was observed from the systems involving 4ClB with Ser, Phe, and Arg.

2.3. Single Crystal X-ray Diffraction (SCXRD)

Single crystals of synthesized derivatives with suitable size and diffracting quality were mounted on nylon loops. The diffraction data were collected on a Supernova diffractometer equipped with a micro-focus X-ray source (MoKα radiation, λ = 0.71073 Å) and an Atlas CCD detector. The collected data were processed with CrysalisPro software (version-171.42.58a; Rigaku Oxford Diffraction: Oxford, UK) [35]. The structures were solved with intrinsic methods and refined by the full-matrix least-squares method on F^2 (ShelxT and ShelxL [36,37] program packages using OLEX2-ver. 1.5 software [38]. All the nonhydrogen atoms were located successfully from the Fourier map and were refined anisotropically. The hydrogen atoms were placed on calculated positions riding on the parent carbon atoms (U_{eq} = 1.2 for C-$H_{aromatic}$ = 0.93 Å and C-$H_{methylenic}$ = 0.97 Å). The N–H

and O–H hydrogen atoms were located on difference Fourier maps and refined isotropically. Ortep-3v2 software [39] was used to prepare the figures. Complete crystallographic data for the structure of compounds **1**–**5** reported in this paper have been deposited in the CIF format with the Cambridge Crystallographic Data Center as 2236720–2236724, respectively.

2.4. Powder X-ray Diffraction (PXRD)

Powder XRD patterns were determined for the physical powder of compounds **1**–**5** to establish crystalline properties, purity, and the eventual presence of polymorphs. Powder samples of the synthesized co-crystals were analyzed on an Empyrean Powder X-ray diffractometer (Malvern Panalytical, Almelo, The Netherlands) in the 2–50° 2θ range using Cu radiation (λ = 1.5406 Å) and PIXcel3D detector. The diffraction patterns of the co-crystals were compared with those of the starting compounds and those computed from SCXRD pattern to confirm the presence or absence of additional phases (Figures S1–S5).

2.5. Thermal Analysis (DSC)

Differential scanning calorimetry was conducted to estimate the thermotropic properties and thermal behaviors of the new co-crystals. DSC analyses were performed on a Discovery DSC250 (TA instruments, New Castle, DE, USA). Samples weighing between 1 and 5 mg were heated in aluminum pans from 20 to 350 °C (10 °C·min^{-1}) in argon (flow rate 10 mL·min^{-1}). The endothermic/exothermic effects of the solvent evaporation, melting point, and decomposition of the synthesized compounds were determined from the DSC experiments.

2.6. Thermogravimetric Analysis (TGA)

The weight loss of a sample as a function of temperature is typically assessed by thermogravimetric analysis (TGA). The TGA was performed on a Q50 analyzer (TA Instruments) using ~10 mg of sample placed in a ceramic crucible. Measurements were made in the temperature range of 20 to 350 °C with a heating rate of 10 °C/min under a nitrogen flow rate of 25 mL/min.

3. Results and Discussion

Although the possible formation of molecular complexes based on 4-halophenylboronic acids has been reported [21], a search in the Cambridge Structural Database [40] (CSD Version 2022.2; August 2022) yielded only 39 structures [12,21,22,41–44] for 4-Halophenylboronic acids (Halo = Cl, Br or I) with eleven structures containing the 4ClB molecule [12,21,43,45]. Of the eleven structures containing the 4-chlorophenylboronic acid, in six the $B(OH)_2$ conformation is *syn*/*anti* (NIQYUI, RORMOC, RORMUI, RORNOD RORPOF, and ULUQUP) and in five (RORMIW, TAZBII, TAZLAK, TAZLEO, and TAZPIW) the conformation is *syn*/*syn.* Similarly, for 4-iodo and 4-bromophenylboronic acid, six structures show *syn*/*syn* conformation, three exhibit simultaneously *syn*/*syn* and *anti*/*anti* conformation, and the remaining eleven have *syn*/*anti* conformation (FETZUA has been excluded due to the improbable position of the hydrogens, while BPHBAC has no H atoms). Compared to the conformational preferences of aromatic boronic acids 81%, 13%, and 6% [22], and 70%, 23%, and 7% (from 240 structures, CSD Version 5.37) for *syn/anti*; *syn/syn*; and *anti/anti* conformations, respectively, in the case of 4-halophenylboronic acids the conformational preferences are not as pronounced (59%, 26% and 15%), with the main conversion occurring for *syn/anti* to *syn/syn*. Nevertheless, the design of the co-crystals acknowledged the domination of the *syn/anti* conformation. The newly obtained co-crystals were characterized by single-crystal analysis and DSC. The most important data collection and refinement parameters for 4ClB:PRO, 4ClB:NIT, 4ClB:ACL, 4ClB:TEO, and 4ClB:CAF are provided in Table 1. The ORTEP view of the molecules in the ASU of compounds **1**–**5** with the appropriate labeling scheme is shown on Figure 1. The structural description of the obtained co-crystals is discussed in the next section.

From the molecular structures (Figure 1), it is evident that the –$B(OH)_2$ moiety of the boronic acid is predominantly in the *syn*/*anti* conformation, with the exception of the 4ClB:PRO supramolecular assembly.

Table 1. The most important data collection and refinement parameters for 4ClB:PRO, 4ClB:NIT, 4ClB:ACL, 4ClB:TEO, and 4ClB:CAF.

Compound	**1**	**2**	**3**	**4**	**5**
	4ClB:PRO	4ClB:NIT	4ClB:ACL	4ClB:TEO	4ClB:CAF
CCDC number	2236720	2236721	2236722	2236723	2236724
Formula	$C_{11}H_{15}BO_4ClN$	$C_{12}H_{12}BClN_4O_6$	$C_{14}H_{17}BClN_5O_5$	$C_{13}H_{14}BClN_4O_4$	$C_{40}H_{44}B_4Cl_4N_8O_{12}$
Formula weight	271.50	354.52	381.58	336.54	1013.87
Temperature/K	290.0 (2)	290.0	290 (2)	290 (2)	290 (2)
Crystal system	monoclinic	triclinic	monoclinic	triclinic	triclinic
Space group	$P2_1$	*P*-1	$P2_1$	*P*-1	*P*-1
a/Å	6.6059 (7)	6.8833 (5)	4.0007 (4)	7.5153 (6)	7.2639 (4)
b/Å	7.7320 (8)	7.2705 (5)	11.0858 (8)	9.4796 (13)	17.9480 (14)
c/Å	13.0643 (13)	17.7274 (9)	19.5865 (13)	11.9034 (8)	20.1908 (14)
α/°	90	93.911 (5)	90	85.806 (8)	115.949 (7)
β/°	102.532 (11)	96.519 (5)	95.837 (7)	80.073 (7)	94.592 (5)
γ/°	90	117.499 (7)	90	68.837 (12)	93.700 (5)
Volume/Å^3	651.38(12)	774.49 (10)	864.17 (12)	778.93 (15)	2344.7 (3)
Z	2	2	2	2	2
ρ_{calcg}/cm^3	1.384	1.520	1.466	1.435	1.436
μ/mm^{-1}	0.298	0.285	0.258	0.270	0.322
F(000)	284.0	364.0	396.0	348.0	1048.0
Crystal size/mm^3	0.25 × 0.24 × 0.2	0.24 × 0.2 × 0.16	0.35 × 0.15 × 0.15	0.35 × 0.3 × 0.15	0.35 × 0.2 × 0.15
Radiation	MoKα (λ = 0.71073)	MoKα (λ = 0.71073)	MoKα (λ = 0.71073)	MoKα (λ = 0.71073)	MoKα (λ = 0.71073)
2Θ range for data collection/°	6.39 to 62.25	6.378 to 61.844	6.272 to 57.708	5.738 to 62.162	5.662 to 58.416
Index ranges	$-9 \le h \le 6$, $-11 \le k \le 7$, $-18 \le l \le 18$	$-9 \le h \le 9$, $-10 \le k \le 9$, $-25 \le l \le 23$	$-4 \le h \le 5$, $-12 \le k \le 13$, $-25 \le l \le 25$	$-9 \le h \le 10$, $-13 \le k \le 12$, $-16 \le l \le 17$	$-9 \le h \le 8$, $-21 \le k \le 24$, $-27 \le l \le 24$
Reflections collected	4160	8671	4180	8481	18,637
Independent reflections/$R_{factors}$	2700 R_{int} = 0.0310, R_{sigma} = 0.0657	4307 R_{int} = 0.0217, R_{sigma} = 0.0386	2899 R_{int} = 0.1390, R_{sigma} = 0.1157	4415 R_{int} = 0.0287, R_{sigma} = 0.0432	10,462 R_{int} = 0.0799, R_{sigma} = 0.1092
Data/restraints/parameters	2700/1/163	4307/0/219	2899/1/242	4415/0/212	10,462/0/639
GOF on F^2	0.952	1.037	1.053	1.061	1.098
Final R indexes *[I> = 2σ (I)]*	R_1 = 0.0550, wR_2 = 0.1233	R_1 = 0.0519, wR_2 = 0.1094	R_1 = 0.0752, wR_2 = 0.1803	R_1 = 0.0599, wR_2 = 0.1682	R_1 = 0.0953, wR_2 = 0.2377
Final R indexes [all data]	R_1 = 0.1223, wR_2 = 0.1551	R_1 = 0.0898, wR_2 = 0.1293	R_1 = 0.0927, wR_2 = 0.2027	R_1 = 0.1009, wR_2 = 0.2029	R_1 = 0.1527, wR_2 = 0.2901
Largest diff. peak/hole/e Å^{-3}	0.17/−0.16	0.28/−0.24	0.28/−0.39	0.30/−0.30	0.88/−0.58

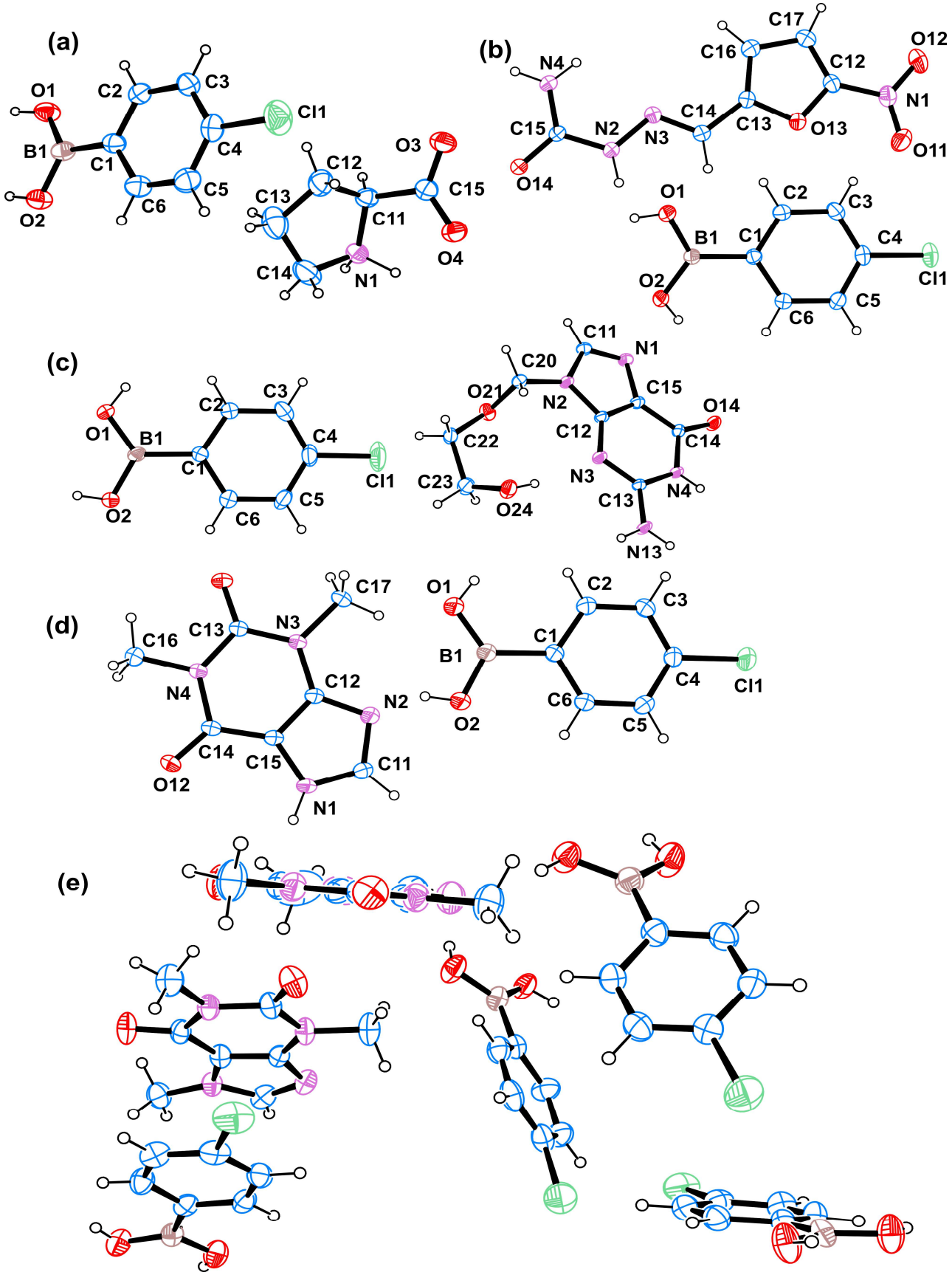

Figure 1. Ortep view of the molecules present in the ASU of (**a**) 4ClB:Pro (1:1), (**b**) 4ClB:NIT (1:1), (**c**) 4ClB:ACL (1:1), (**d**) 4ClB:TEO (1:1), and (**e**) 4ClB:CAF (2:1).

Co-crystals of compound **1** 4ClB:PRO were obtained from the 1:1 molar ratio of 4ClB:PRO from the water/ethanol solution (1:1 v/v). The crystal structure of 4ClB:Pro is isostructural to LOXHAJ [41] with structure similarity parameters: S = 0.0165, $d_{max.}$ = 0.5985 (Å), $d_{av.}$ = 0.2911 (Å), Δ = 0.111 [46,47] (after transforming **1** with (P, p): $-c,-b,-a$; 0, −0.77209, −1/2), COMPSTRU [47,48]. The difference in the relative position of the Cl and I atoms is 0.1721 Å. As one would expect, the –$B(OH)_2$ group in structure **1** (4ClB:PRO) is in *syn*/*syn* conformation. Thus, the hydrogen bonding between $B(OH)_2$ groups is prohibited, due to the fact that steric hindrance and the hydrogen bonding occur between the proline carboxylic group and the –$B(OH)_2$ moiety from 4ClB. In the crystal structure, the proline molecule is present as a zwitterion. The transfer of a proton from COO^- to NH_2^+ results in a tetrahedral conformation of the N (sp^3 hybridization), allowing the two hydrogen atoms of NH_2^+ to interact with the available acceptors from the $B(OH)_2$ and COO^- groups. The result is the observation of three more hydrogen bonding interactions (Figure 2 and Table 2). Previous studies suggested that the formation of the anionic –$B(OH)_2$ ... –OOC– heterosynthon is energetically more favorable than the –$B(OH)_2$ ... HOOC– $R_2^2(8)$ motif [49,50].

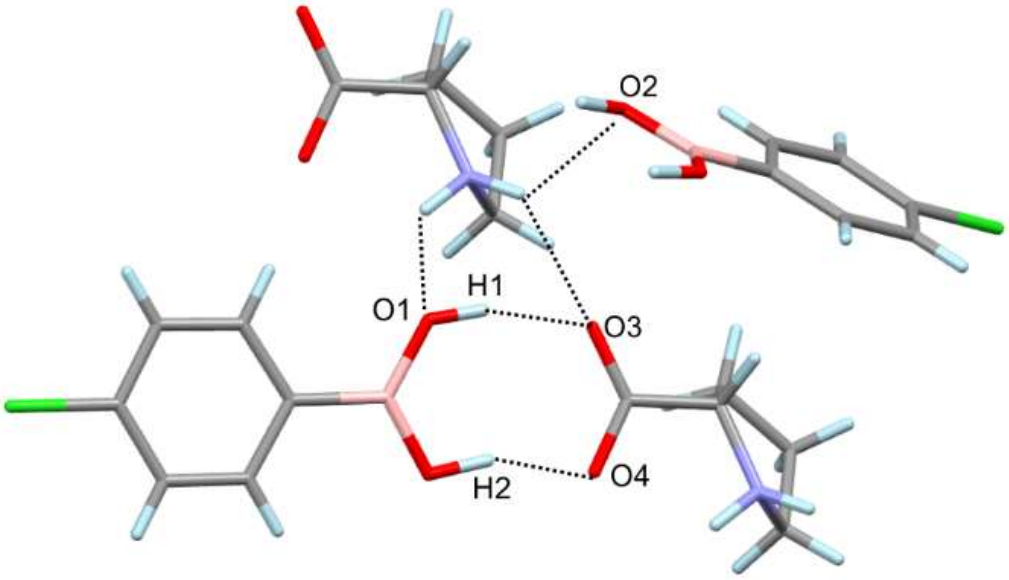

Figure 2. Observed hydrogen bonding interactions (shown as dotted lines) in **1**.

Table 2. Observed weak interactions in **1**.

D	H	A	d(D-H)/Å	d(H-A)/Å	d(D ... A)/Å	D-H-A/°
O1	H1	O3 [1]	0.94	1.77	2.672 (5)	159.7
O2	H2	O3 [1]	0.98	2.64	3.460 (5)	142.0
O2	H2	O4 [1]	0.98	1.66	2.589 (5)	158.0
N1	H1A	O1 [2]	1.03	2.20	3.050 (5)	138.2
N1	H1A	O4	1.03	2.03	2.616 (5)	113.4
N1	H1B	O2 [3]	0.89	2.29	2.924 (5)	127.6
N1	H1B	O3 [4]	0.89	2.47	3.205 (5)	140.8

[1] $-1+x,+y,-1+z$; [2] $+x,+y,1+z$; [3] $-x,-1/2+y,1-z$; [4] $-1+x,+y,+z$.

Further analysis of the close contacts present in the crystal structure of 4ClB:PRO revealed that the chlorine atom is not involved in weak interactions. A somewhat distorted T-type C–H ... π interaction (3.289 Å) is observed between the phenyl rings (Figure 3).

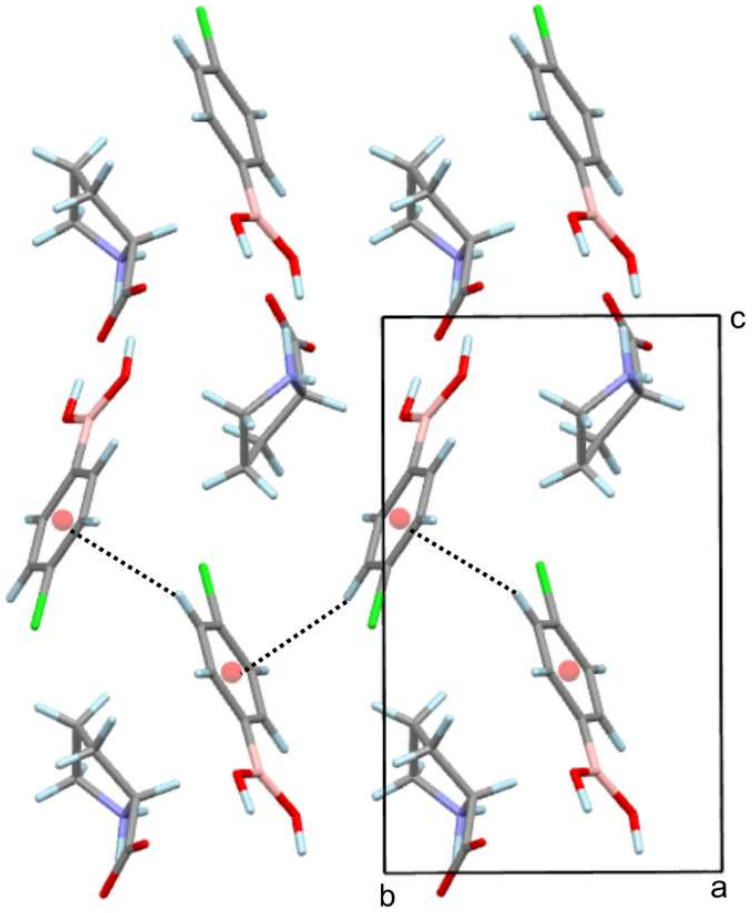

Figure 3. Three-dimensional arrangement of the molecules in **1** producing a T-type C–H ... π interaction (3.289 Å) between phenyl rings.

In view of the almost identical hydrogen bonding interactions observed in LOXHAJ and **1**, this is a clear example of the potential of 4-haloboronic acids for isostructural design.

Interestingly, co-crystallization trials involving 4ClB and the amino acids (AA) Ser, Phe, and Arg were unsuccessful. It is interesting to point out that the co-crystallization cannot be related to the variation in common AA descriptors such as the pK_a and pK_b values (from the used AA, only Arg has pKx side chains), hydrophobicity/hydrophilicity (Pro and Arg are hydrophobic, Ser neutral, and Phe hydrophylic), etc.

The DSC thermograms of compound **1**, proline hydrate and 4-chlorophenylboronic acid, are shown on Figure 4a. The comparison of the observed endothermic effects (e.g., temperature) reveals that that the co-crystal thermal comportment is different from that of the two starting compounds. The DSC of proline shows two endothermic effects at ~56 and 228 °C. The first effect can be associated with the release of the water molecules. This is supported by the TGA analysis registering ~14% losses corresponding to one molecule of water (Figure 4b). The second endothermic effect is the melting of the proline followed by decomposition (broad peak at 235 °C). The 4-chlorophenylboronic acid thermogram displays only one effect at ~295 °C associated with the melting of the substance. The DSC of the co-crystal between 4-chlorophenylboronic acid and proline discloses also only endothermic effects. The first and second ones are detected at 66 and 117 °C, but the TGA does not register weight losses. Thus, those effects can be related to destruction of the co-crystal and some molecular rearrangements. The melting of the co-crystals is observed at 252 °C and is accompanied by significant weight losses (Figure 4b).

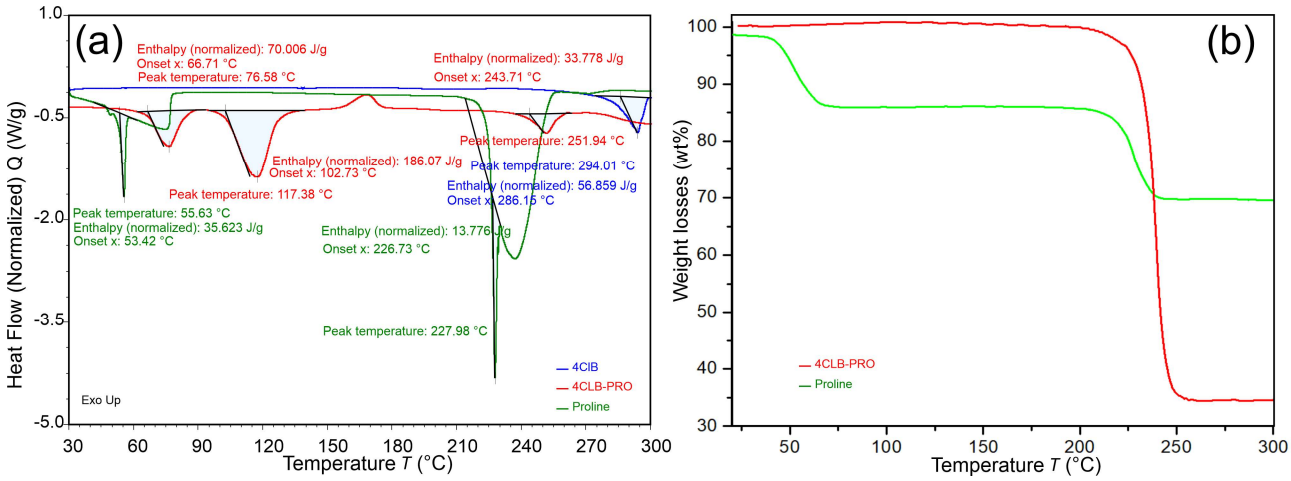

Figure 4. DSC thermograms of (**a**) compound **1** (red), proline (green), and 4-chlorophenylboronic acid (blue) showing the endothermic effects and (**b**) TGA of compound **1** and proline hydrate.

Co-crystals of compound **2** (4ClB:NIT) were obtained from a 2:1 molar ratio of 4ClB:NIT from a water/ethanol solution (1:1 v/v). Nitrofurazone (Furacilin, nitrofural) is a compound with bactericidal properties [51]. Molecules of 4CLB and NIT co-crystallize in the $P\bar{1}$ space group with one molecule NIT and one molecule 4CLB in the asymmetric unit. The angle between the mean planes of the $B(OH)_2$ group and the benzyl ring is 15.67 (8)°. The NIT molecule is nearly planar with *rmsd* of 0.031 Å. The hydrogen atoms of the $-B(OH)_2$ group in the structure **2** are in *syn*/*anti* conformation, and thus adjacent 4CLB molecules produce the $R_2^2(8)$ motif (Figure 4 and Table 3), typical for boronic acids. NIT molecules also produce a $R_2^2(8)$ motif through the amide group. The homodimmers of 4CLB and NIT interact "laterally" through N3-H3 ... O1 and O2-H2 ... O14 = C15 (Figure 4 and Table 3). The NO_2 group and the Cl atom are facing each other, and a typical halogen bonding interaction NO_2 ... Cl (3.165 Å) is detected [52,53]. In addition, the three-dimensional arrangement of the molecules in the crystal structure shows that the 4CLB and NIT molecules are positioned on top of each other; thus, Cl δ^+ interacts with O^- while Cl δ^- is compensated by the nitro group N^+ (Figure 5). The three-dimensional arrangement of the molecules of 2 (Figure 6) is such that no suitable acceptor is available for the second hydrogen (H4B) of the amide moiety.

Table 3. Observed hydrogen and weak interactions in **2**.

D	H	A	d(D-H)/Å	d(H-A)/Å	d(D-A)/Å	D-H-A/°
O2	H2	O14 [1]	0.82	2.01	2.7821 (19)	155.7
O1	H1	O2 [1]	0.82	1.99	2.8019 (19)	170.8
N3	H3	O1	0.86	2.55	3.244 (2)	139.0
N3	H3	O14 [2]	0.86	2.39	3.030 (2)	131.2
N3	H3	O2	0.86	2.838	3.351 (3)	120.1
N4	H4A	O14 [3]	0.86	2.05	2.911 (2)	174.7
Cl1	-	O12	-	3.165	-	-

[1] $2-x, 2-y, 2-z$; [2] $2-x, 1-y, 2-z$; [3] $3-x, 1-y, 2-z$.

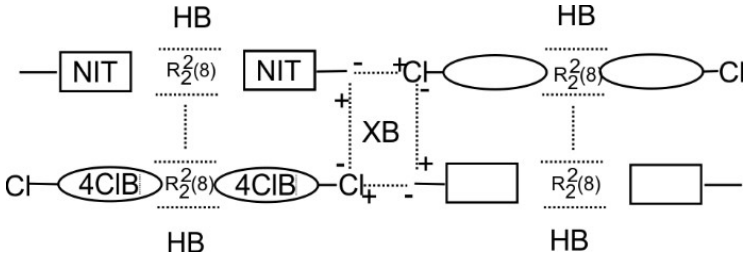

Figure 5. Scheme of the weak interactions and resulting packing in the crystal structure of **2**, HB hydrogen bonding, and XB halogen bonding.

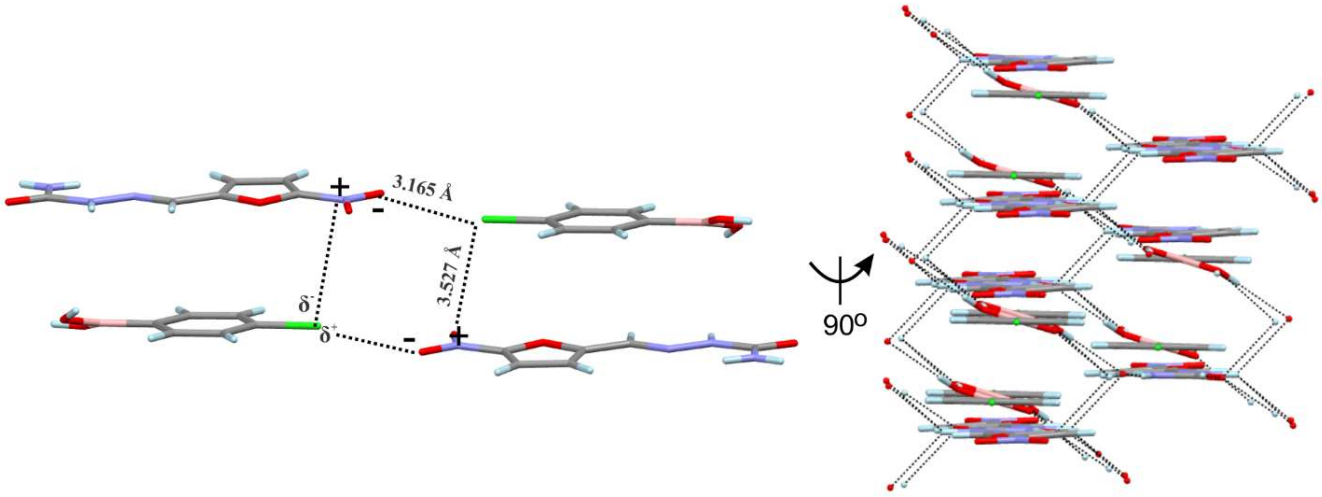

Figure 6. Arrangement of the 4ClB and NIT molecules in the crystal structure of **2**; the hydrogen and halogen bonding interactions are shown as dotted lines.

The comparison of the recorded powder diffraction pattern of the 4ClB:NIT and that calculated from the SCXRD data (Figure S2) reveals the presence of additional reflections, clearly discernible at 8.73, 8.82, 8.96, 18.5, and 18.8° 2θ in the PXRD. The additional reflections cannot be related to the diffraction resulting from known phases of the starting compounds Nitrofurazone (WERVEU01, WERVEU02, and 00-047-2223), 4-chlorophenylboronic acid (NIQYUI), or unindexed patterns present in the ICDD, e.g., 00-015-1133 and 00-033-1787. As Nitrofurazone shows a tendency to produce polymorphs, it is possible that a co-crystal with another molecular geometry of the NIT molecule may be produced.

The DSC thermograms of compound **2**, Nitrofurazone and 4-chlorophenylboronic acid, are shown in Figure 7a,c. The comparison of the observed endothermic and exothermic effects (e.g., temperature) reveals that that the co-crystal thermal comportment is different from that of the two starting compounds. The DSC of Nitrofurazone shows one exothermic associated with the sublimation and supported by TGA (Figure 7d). The 4-chlorophenylboronic acid thermogram displays one effect at ~295 °C associated with the melting of the substance. The DSC of the co-crystal between 4-chlorophenylboronic acid and Nitrofurazone discloses endothermic effects at ~58 and 107 °C; the first one is sharp and relatively weak compared to the second one. In this temperature range, the TGA does not detect weight losses; thus, the endothermic effects are again related to the destruction of the co-crystal. The last maximum is exothermic with a maximum at 238 °C, and by association the sublimation of the Nitrofurazone as TGA registers significant weight losses (Figure 7b).

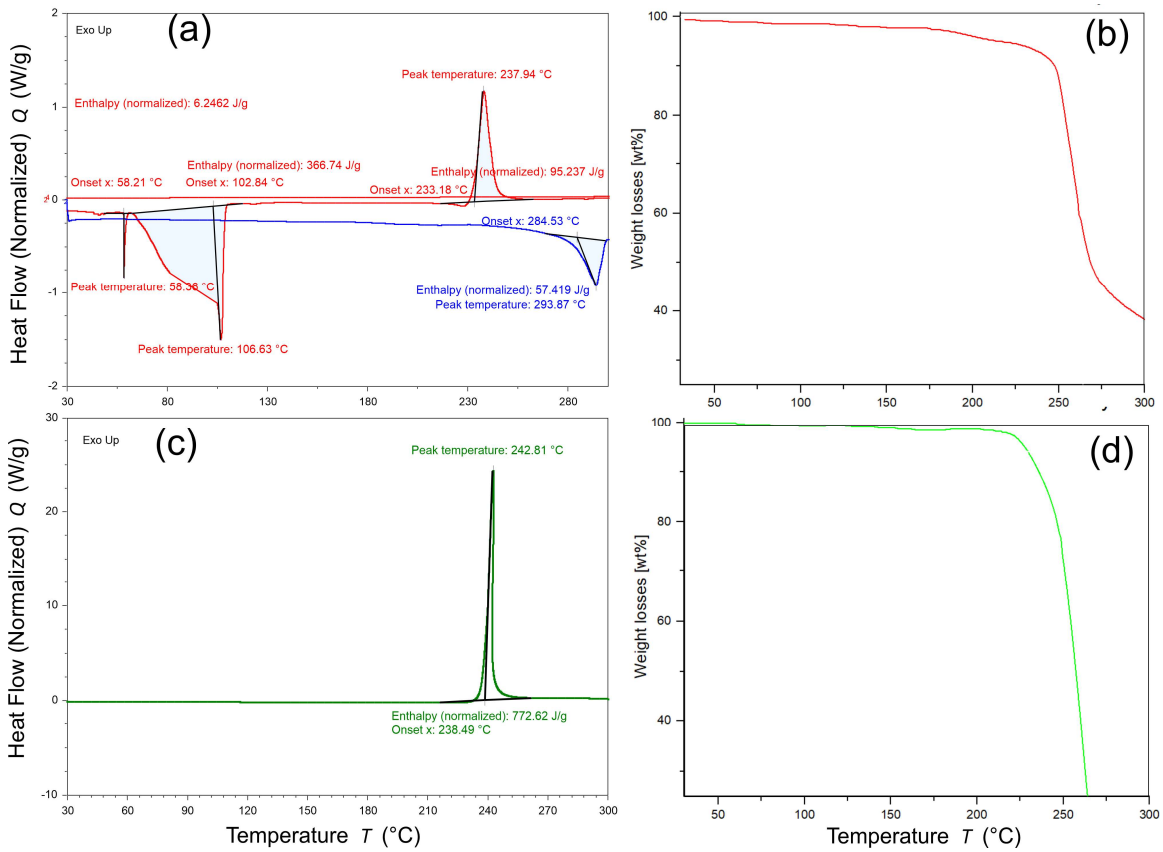

Figure 7. DSC thermograms of (**a**) compound **2** (red), nitrofurazone (green), and (**c**) 4-chlorophenylboronic acid (blue) showing the endothermic and exothermic effects; TGA of (**b**) compound **2** and (**d**) nitrofurazone.

Co-crystals of compound **3** (4ClB:ACL) were obtained from a 1:1 molar ratio of 4ClB:ACL from water/ethanol solution with a solvent ratio of 1:1 v/v. The co-crystal of 4ClB:ACL (monoclinic, space group $P2_1$) contains one molecule of ACL and one molecule of 4ClB in the ASU. The $B(OH)_2$ group in structure 3 is in *syn*/*anti* conformation. The observed hydrogen bonding reveals an intramolecular hydrogen bond for the ACL molecule. Homosynthons of ACL produce zigzag chains ($R_2^2(9)$ motif) (Figure 8a), and in order to obtain the densest packing, 4ClB molecule positions in the side groove of the chains. The $B(OH)_2$ moiety takes part in the hydrogen bonding stabilization while the R–Cl points towards the open space. Thus, the 4ClB of the different chains intertwine, and a halogen bond (Cl . . . H23A-C23 of 2.955 Å) between 4CLB and ACL produces pseudo-layers (Figure 8b).

The DSC thermograms of compound **3**, aciclovir and 4-chlorophenylboronic acid, are shown in Figure 10a. The comparison of the observed endothermic effects (e.g., temperature) reveals that that the co-crystal thermal comportment is different from that of the two starting compounds. The DSC of aciclovir shows one well-visualized endothermic effect at ~255 °C related to the melting of ACL. The decomposition of ACL accompanies the melting, although it finishes after the melting, as seen in Figure 10. The 4-chlorophenylboronic acid thermogram displays one effect at ~294 °C associated with the melting of the substance. The DSC of the co-crystal between the 4-chlorophenylboronic acid and the aciclovir discloses also only endo effects but at lower temperatures. The first endothermic effect is complex, with a sharp maximum at ~99 °C. At the same temperature, no effects are detected for 4CLB and ACL. Interestingly, the TGA of compound **3** reveals weight losses starting at 30 °C and finishing after ~100 °C. The weight losses are related to at least two steps of the TGA curve (Figure 10b). Thus, the destruction and melting at 99 and 112 °C, respectively, of the 4CLB-ACL co-crystal occur at lower temperatures than those of 4CLB-PRO and 4CLB-NIT.

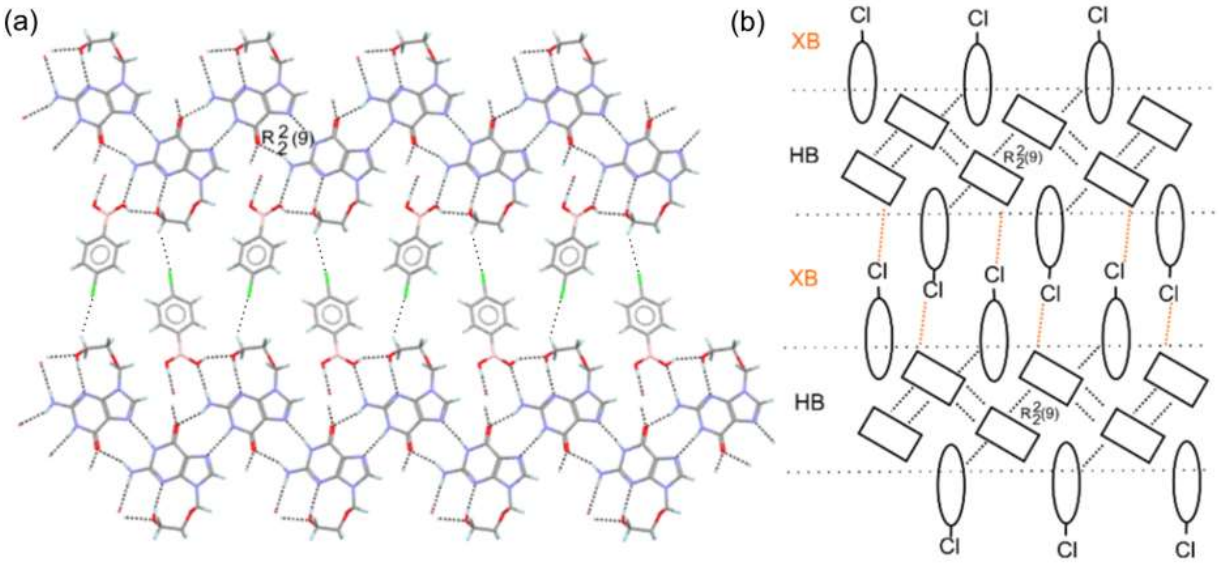

Figure 8. Visualization of (**a**) the hydrogen and halogen bonding interaction in **3** and (**b**) schematic of the pseudo-layer construction.

In addition to the abovementioned HB and XB interactions, C-H . . . O and C-H . . . π interactions are responsible for the stacking of the molecules (Figure 9), i.e., the pseudo layers are stacked.

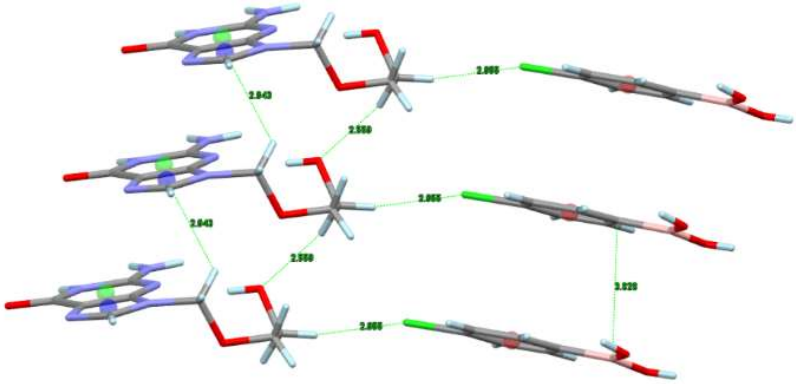

Figure 9. Observed weak C-H . . . O and C-H . . . π interactions in **3**.

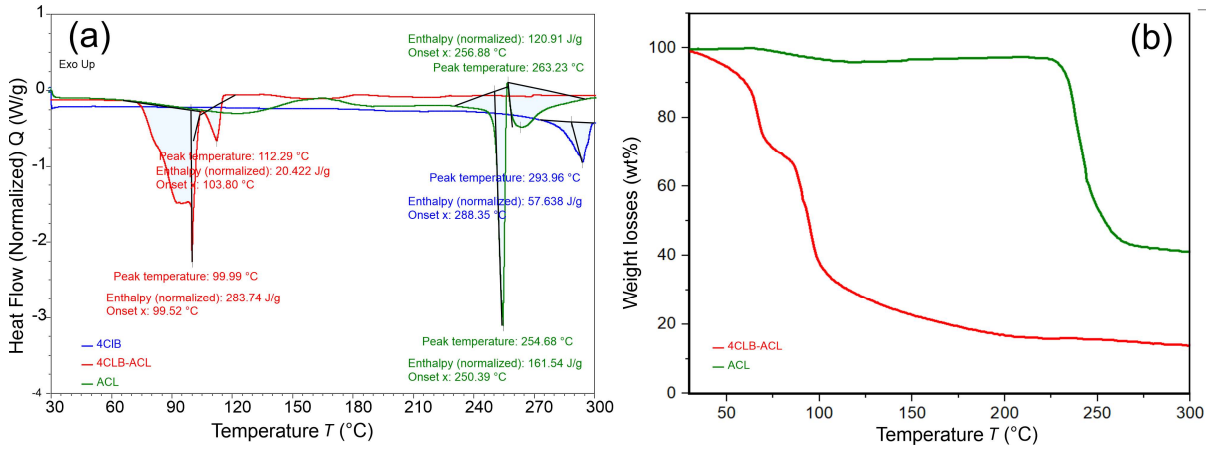

Figure 10. DSC thermogram of (**a**) compound **3** (green), aciclovir (red), and 4-chlorophenylboronic acid (blue) showing the endothermic effects and (**b**) TGA of compound **3** and aciclovir.

Co-crystals of compound **4** (4ClB:TEO) were obtained by Shimpi et al. [43] from a 1:1 molar ratio of 4ClB:TEO and by slow evaporation of an ethanol solution. In the present study, the co-crystals were obtained in a similar way, e.g., 1:1 molar ratio of 4ClB:TEO, but with a water/ethanol solution (1:1 v/v ratio). The co-crystal of 4CLB:TEO (Triclinic, $P\bar{1}$ space group) is isostructural to the one reported by Shimpi et al. [43], and the $B(OH)_2$ group in the structure of **4** is also in *syn/anti* conformation. The observed weak interactions in **4** are in accordance with the previously reported structure of 4ClB:TEO [43] and follow the suggested in [21] reproducible characteristics of noncovalent bonds in 4-halophenylboronic acids. Briefly, intermolecular hydrogen bonds are observed between $B(OH)_2$ moiety and the imidazole N atoms and carbonyl O atoms of the TEO molecule, forming a ring (void). Intermolecular hydrogen bonds (N1H1 ... O12) are present between adjacent TEO molecules, producing a $R_2^2(10)$ motif (Figure 11).

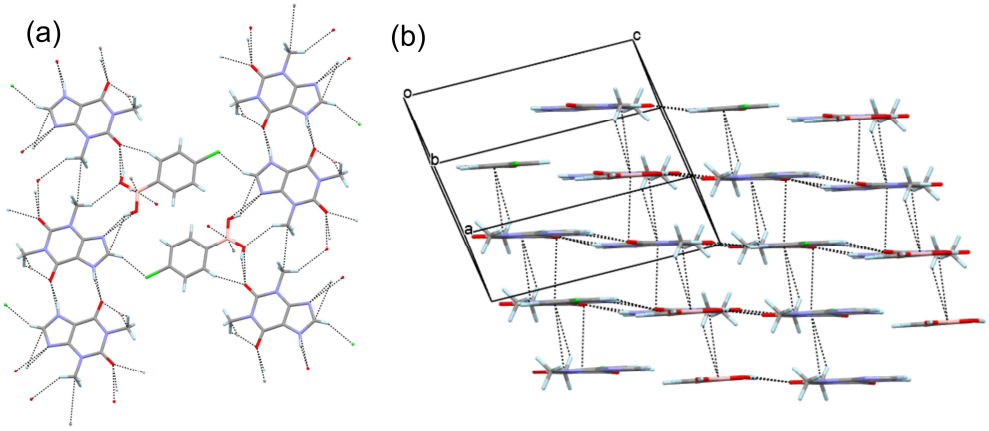

Figure 11. Visualization of (**a**) the hydrogen and halogen bonding interaction in **4** and (**b**) the pseudo-layer construction based on hydrogen bonding and π .... π interactions.

The DSC thermograms of the co-crystal **4**, theophylline and 4-chlorophenylboronic acid, are shown in Figure 12a. The DSC is quite similar to that of compound **3**, where the starting compounds melt at higher temperatures, while the co-crystal exhibits endothermic effects (~59 and ~76 °C) and presumably melting at lower temperatures. Indeed, TEO and 4CLB melting occurs at 271 and 291 °C, respectively, while the highest endothermic effect for **4** is registered ~240 °C. The TGA of Theophylline (Figure 5b) registers only weight losses associated with the melting. On the other hand, the TGA of the co-crystal 4CLB-TEO reveals ~6% weight losses up to 60 °C and additional 35% weigh loss in the 150–200 °C range and finally in the 220–300 °C range.

Co-crystals of compound **5** (4ClB:CAF) were obtained from a 2:1 molar ratio of 4ClB:CAF from a water/ethanol solution (1:1 v/v ratio). The co-crystal of 4ClB:CAF (Triclinic, $P\bar{1}$ space group) contains two molecules of CAF and four molecules of 4CLB in the ASU. The overlay of the four molecules 4CLB discloses a conserved geometry (rmsd of 0.120 to 0.310 Å), as only the angle between the mean planes of the aromatic ring and the $-B(OH)_2$ moieties slightly varies (from 5.00 to 28.35°). In the case of the two CAF molecules, the situation is similar, with rmsd of 0.254 Å. Although all of the $-B(OH)_2$ groups in **5** are in *syn/anti* conformation, the 4CLB molecule hydrogen bonding interaction is different. Two of the 4CLB molecules produce dimers through the expected $R_2^2(8)$ interaction, while the other two molecules along with the caffeine ones produce $R_4^4(20)$ rings (Figure 13). All the available donors and acceptors are involved in the hydrogen bonding; however, the crystal packing is additionally stabilized by a multitude of weak C-H ... O and π ... π interactions (Table 4).

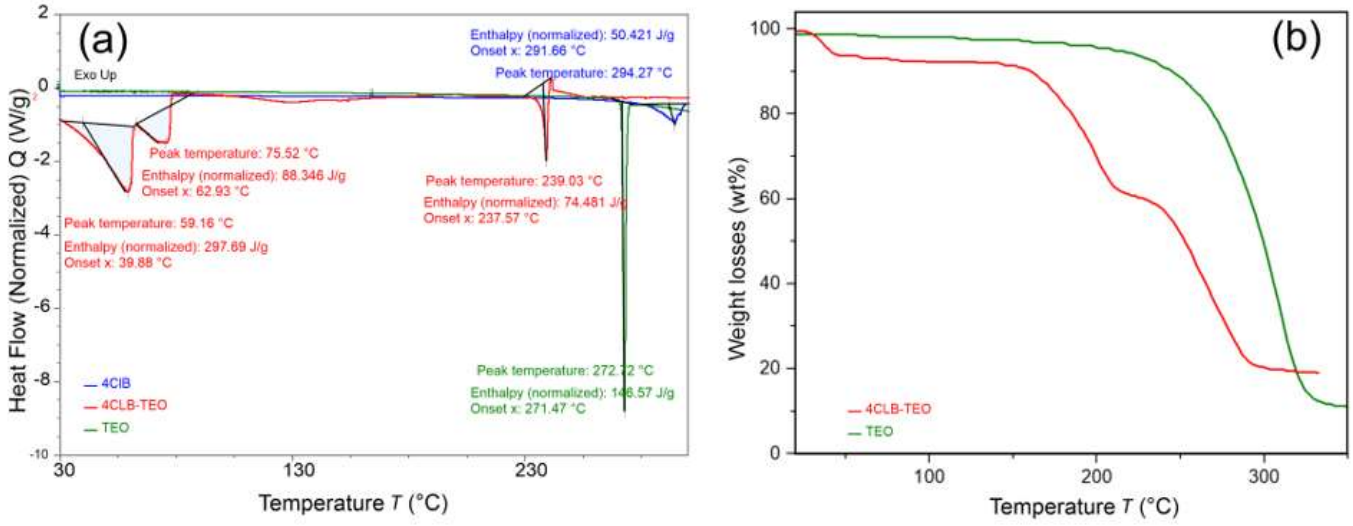

Figure 12. DSC thermogram of (**a**) compound **4** (green), theophylline (red), and 4-chlorophenylboronic acid (blue) showing the endothermic effects and (**b**) TGA of compound **4** and theophylline.

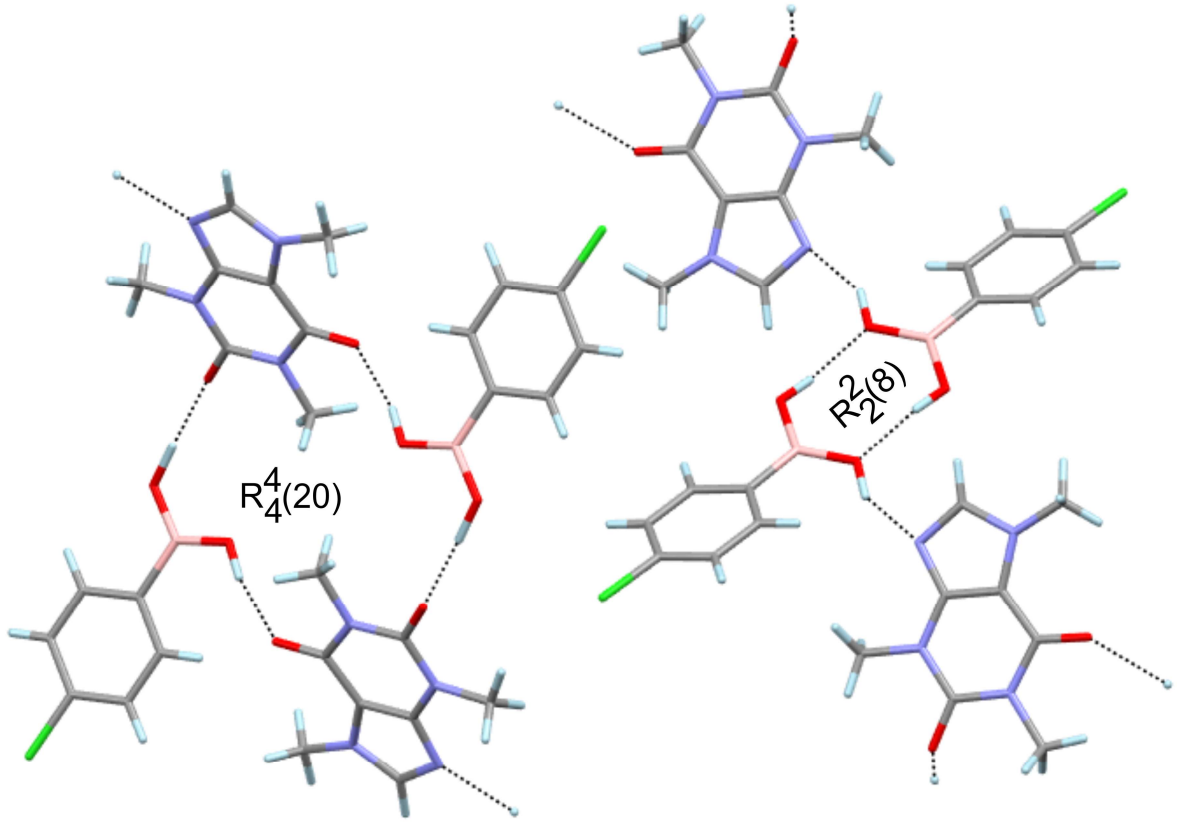

Figure 13. Visualization of the different hydrogen bonding interaction of the $-B(OH)_2$ moiety in **5**.

Table 4. Observed hydrogen and weak interactions in **5**.

D	H	A	d(D-H)/Å	d(H-A)/Å	d(D-A)/Å	D-H-A/°
O42	H42	O62 [1]	0.82	2.07	2.826 (5)	153.9
O21	H21	N53 [2]	0.82	2.02	2.796 (5)	157.4
O11	H11	O12 [3]	0.82	1.95	2.754 (5)	167.2
O32	H32	O51 [4]	0.82	1.96	2.729 (4)	154.8
C66	H66B	O41 [5]	0.96	2.58	3.510 (6)	163.8
C58	H58B	Cl31 [6]	0.96	2.98	3.910 (5)	164.3
C58	H58C	O41 [7]	0.96	2.60	3.436 (6)	145.8
C68	H68A	O31 [8]	0.96	2.51	3.352 (8)	146.6
C68	H68B	Cl41 [7]	0.96	2.88	3.494 (6)	122.8
C68	H68C	O61	0.96	2.63	3.123 (9)	112.3
O41	H41	O61 [5]	0.75 (4)	2.11 (4)	2.833 (5)	164 (4)
O22	H22	O21 [9]	0.74 (5)	2.09 (5)	2.829 (5)	171 (5)
O31	H31	O52 [8]	1.08 (6)	1.75 (6)	2.814 (5)	164 (5)
O12	H12	N63	0.89 (6)	2.01 (6)	2.793 (5)	146 (5)

[1] $1+x, -1+y, +z$; [2] $-x, -y, 1-z$; [3] $-1-x, 1-y, 1-z$; [4] $+x, +y, -1+z$; [5] $1-x, 1-y, 2-z$; [6] $1-x, -y, 1-z$; [7] $-1+x, +y, +z$; [8] $1-x, 1-y, 1-z$; [9] $-1-x, -y, 1-z$.

The DSC thermograms of compound **5**, caffeine and 4-chlorophenylboronic acid, are shown in Figure 14a. The DSC is quite similar to that of compound **3** and **4**, e.g., the starting compounds CAF and 4CLB exhibit melting at higher temperatures (at 237 and 291 °C, respectively) accompanied by weight losses (Figure 14b), while the co-crystals exhibit endothermic effects at lower temperatures. Indeed, the DSC of the co-crystal **5** displays four endothermic effects (~66, 82, 88, and ~102 °C) attributed to the destruction of the co-crystal and the readjustment of the molecular geometries.

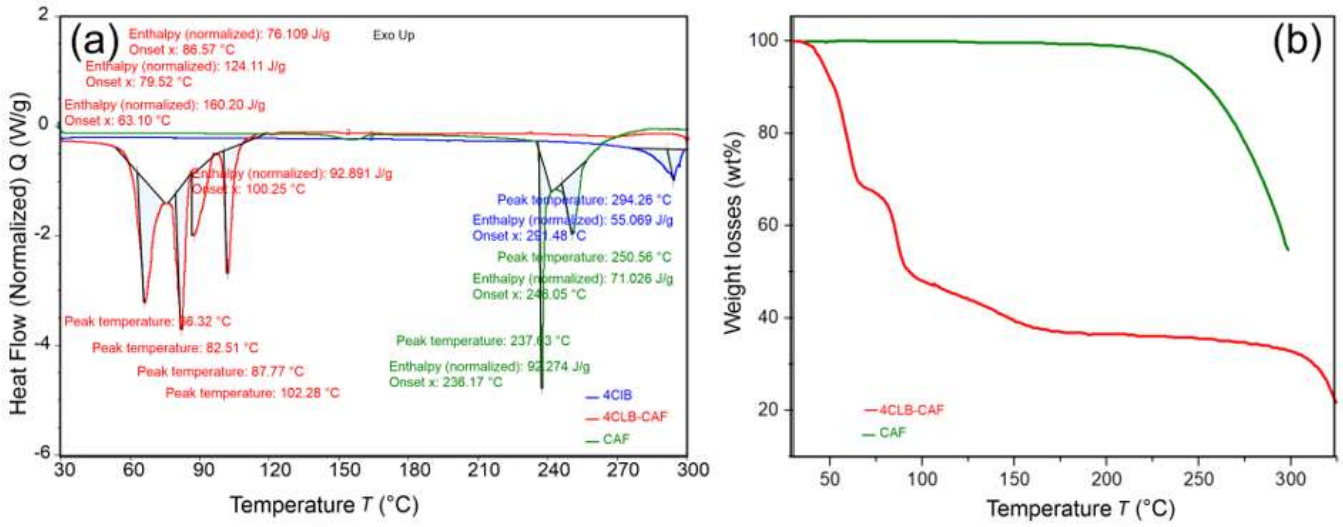

Figure 14. DSC thermogram of (**a**) compound **5** (green), caffeine (red), and 4-chlorophenylboronic acid (blue) showing the endothermic effects and (**b**) TGA of compound **5** and caffeine.

The co-crystallization trials of 4CLB: Diltiazem, Paracetamol, Indometacine, Serine, Phenylalanine, and Arginine did not lead to the formation of co-crystals, at least for the attempted conditions. The attempts produced a mixture of crystal and amorphous phases (usually with amino acids), two crystal phases of starting compounds, e.g., 4CLB and Paracetamol, and in some more than two crystalline phases were produced when crystal solvates are also formed.

4. Conclusions

In summary, for the first time the synthesis of new 4-chlorophenylboronic acid co-crystals with pharmaceutically acceptable conformers—such as nitrofurazone, aciclovir, and caffeine in different stoichiometry (1:1 and 2:1)—were obtained by the slow evaporation solution growth technique, and the results were reported. The chemical characteristics of the co-crystals were confirmed by single crystal X-ray diffraction and by the powder XRD and DSC techniques. The analysis of packing and interactions in the crystal lattice revealed that molecules in the target co-crystals trough are formed on the basis of the preferred *syn*/*anti* $B(OH)_2$ conformation. Only in one of the five investigated cases was the $B(OH)_2$ in *syn*/*syn* conformation. The single-crystal X-ray diffraction study did not reveal the existence of the characteristic $–B(OH)_2$ hydrogen bond motif in the structures; on the contrary, $R_2^2(8)$ was detected in **2** and **5**, $R_2^2(9)$ in **3**, $R_2^2(10)$ in **4,** and $R_4^4(20)$ in **5**. The weak $\pi \ldots \pi$ and C-H ... O interactions additionally stabilizing the three-dimensional crystal packing were observed in all the structures. The C-H ... Cl or N-H ... Cl halogen interactions were consistently observed in all of the structures. It was shown that DSC analyses may be applied to detect the formation of co-crystals. For all five co-crystals, the DSC thermogram was significantly different than that of the initial reactants. The DSC of the co-crystals was characterized by endothermic effects at lower temperatures (below 100 °C) not present in the initial compounds.

Supplementary Materials: The following supporting information can be downloaded at: https://www.mdpi.com/article/10.3390/cryst13030468/s1, Figures S1–S5: Comparison of powder diffractogram and calculated from single crystal data for compounds **1**–**5**.

Author Contributions: Conceptualization, H.S.-D., V.D. and B.S.; Formal analysis, H.S.-D., V.D. and B.S.; Visualization, H.S.-D., V.D., K.I. and B.S.; Investigation (PXRD), H.S.-D., K.I. and B.S.; Investigation (single crystal), H.S.-D., V.D. and B.S.; (DSC), H.S.-D., V.D. and K.I.; methodology, H.S.-D., V.D. and B.S.; writing—original draft, H.S.-D., V.D., K.I. and B.S.; Funding acquisition, H.S.-D. and B.S. All authors have read and agreed to the published version of the manuscript.

Funding: This research was funded by EU Structural and Social Funds, via BG Programme "Science and Education for Smart Growth": project BG05M2OP001-1.002-0005, "Personalized Innovative Medicine (PERIMED)" (2018–2023).

Data Availability Statement: Complete crystallographic data for the structures reported in this paper have been deposited in the CIF format, and the complete crystallographic data for the structures of compounds **1**–**5** reported in this paper have been deposited in the CIF format with the Cambridge Crystallographic Data Center as 2236720, 2236721, 2236722, 2236723, and 2236724. These data can be obtained free of charge via http://www.ccdc.cam.ac.uk/conts/retrieving.html, deposited on 15 June 2022 (or from the CCDC, 12 Union Road, Cambridge CB2 1EZ, UK; Fax: +441223336033; E-mail: deposit@ccdc.cam.ac.uk).

Acknowledgments: The authors acknowledge the technical support from the project BG05M2OP001-1.002-0005, "Personalized Innovative Medicine (PERIMED)" (2018–2023) (2018–2023).

Conflicts of Interest: The authors declare no conflict of interest.

References

1. Desiraju, G.R. Crystal Engineering: From Molecule to Crystal. *J. Am. Chem. Soc.* **2013**, *135*, 9952–9967. [CrossRef] [PubMed]
2. Bernstein, J. Molecular crystals—Pinching polymorphs. *Nat. Mater.* **2005**, *4*, 427–428. [CrossRef] [PubMed]
3. Bond, A.D. Polymorphism in molecular crystals. *Curr. Opin. Solid State Mater. Sci.* **2009**, *13*, 91–97. [CrossRef]
4. Bernstein, J. *Polymorphism in Molecular Crystals*; Oxford University Press: New York, NY, USA, 2002; p. 14.
5. Bernstein, J.; Davey, R.J.; Henck, J.O. Concomitant polymorphs. *Angew. Chem. Int. Ed.* **1999**, *38*, 3440–3461. [CrossRef]
6. Takale, B.S.; Kong, F.-Y.; Thakore, R.R. Recent Applications of Pd-Catalyzed Suzuki–Miyaura and Buchwald–Hartwig Couplings in Pharmaceutical Process Chemistry. *Organics* **2022**, *3*, 1–21. [CrossRef]
7. Oka, N.; Yamada, T.; Sajiki, H.; Akai, S.; Ikawa, T. Aryl Boronic Esters Are Stable on Silica Gel and Reactive under Suzuki–Miyaura Coupling Conditions. *Org. Lett.* **2022**, *24*, 3510–3514. [CrossRef]
8. Gosecki, M.; Gosecka, M. Boronic acid esters and anhydrates as dynamic cross-links in vitrimers. *Polymers* **2022**, *14*, 842. [CrossRef]

9. Vancoillie, G.; Hoogenboom, R. Synthesis and polymerization of boronic acid containing monomers. *Polym. Chem.* **2016**, *7*, 5484–5495. [CrossRef]
10. Kubo, Y.; Nishiyabu, R.; James, T.D. Hierarchical supramolecules and organization using boronic acid building blocks. *Chem. Commun.* **2015**, *51*, 2005–2020. [CrossRef]
11. Varughese, S.; Azim, Y.; Desiraju, G.R. Molecular complexes of alprazolam with carboxylic acids, boric acid, boronic acids, and phenols. Evaluation of supramolecular heterosynthons mediated by a triazole ring. *J. Pharm. Sci.* **2010**, *99*, 3743–3753. [CrossRef]
12. Georgiou, I.; Kervyn, S.; Rossignon, A.; De Leo, F.; Wouters, J.; Bruylants, G.; Bonifazi, D. Versatile self-adapting boronic acids for H-bond recognition: From discrete to polymeric supramolecules. *J. Am. Chem. Soc.* **2017**, *139*, 2710–2727. [CrossRef] [PubMed]
13. James, T.D.; Phillips, M.D.; Shinkai, S. *Boronic Acids in Saccharide Recognition*; Royal Society of Chemistry: Cambridge, UK, 2006.
14. Valdes-García, J.; Zamora-Moreno, J.; Salomón-Flores, M.K.; Martínez-Otero, D.; Barroso-Flores, J.; Yatsimirsky, A.K.; Bazany-Rodríguez, I.J.; Dorazco-González, A. Fluorescence Sensing of Monosaccharides by Bis-boronic Acids Derived from Quinolinium Dicarboxamides: Structural and Spectroscopic Studies. *J. Org. Chem.* **2023**, *88*, 2174–2189. [CrossRef] [PubMed]
15. Wang, X.; Zhang, W.; Wen, T.; Miao, H.; Hu, W.; Liu, H.; Lei, M.; Zhu, Y. Design and discovery of novel dipeptide boronic acid ester proteasome inhibitors, an oral slowly-released prodrug for the treatment of multiple myeloma. *Eur. J. Med. Chem.* **2023**, *250*, 115187. [CrossRef] [PubMed]
16. Abeysinghe, R.T.; Ravenscroft, A.C.; Knowlden, S.W.; Akhmedov, N.G.; Dolinar, B.S.; Popp, B.V. Synthesis of Novel Multifunctional bora-Ibuprofen Derivatives. *Inorganics* **2023**, *11*, 70. [CrossRef]
17. Moumbock, A.F.; Tran, H.T.; Lamy, E.; Günther, S. BC-11 is a covalent TMPRSS2 fragment inhibitor that impedes SARS-CoV-2 host cell entry. *Arch. Pharm.* **2023**, *356*, 2200371. [CrossRef]
18. Farfán-García, E.D.; Kilic, A.; García-Machorro, J.; Cuevas-Galindo, M.E.; Rubio-Velazquez, B.A.; García-Coronel, I.H.; Estevez-Fregoso, E.; Trujillo-Ferrara, J.G.; Soriano-Ursúa, M.A. Antimicrobial (viral, bacterial, fungal, and parasitic) mechanisms of action of boron-containing compounds. In *Viral, Parasitic, Bacterial, and Fungal Infections*; Elsevier: Amsterdam, The Netherlands, 2023; pp. 733–754.
19. Hoenke, S.; Brandes, B.; Csuk, R. Non-cytotoxic aza-BODIPY triterpene conjugates to target the endoplasmic reticulum. *Eur. J. Med. Chem. Rep.* **2023**, *7*, 100099. [CrossRef]
20. Pedireddi, V.R.; Seethalekshmi, N. Boronic acids in the design and synthesis of supramolecular assemblies. *Tetrahedron Lett.* **2004**, *45*, 1903–1906. [CrossRef]
21. Shimpi, M.R.; SeethaLekshmi, N.; Pedireddi, V.R. Supramolecular architecture in some 4-halophenylboronic acids. *Cryst. Growth Des.* **2007**, *7*, 1958–1963. [CrossRef]
22. Varughese, S.; Sinha, S.B.; Desiraju, G.R. Phenylboronic acids in crystal engineering: Utility of the energetically unfavorable syn,syn-conformation in co-crystal design. *Sci. China Chem.* **2011**, *54*, 1909–1919. [CrossRef]
23. Stazi, M.; Lehmann, S.; Sakib, M.S.; Pena-Centeno, T.; Büschgens, L.; Fischer, A.; Weggen, S.; Wirths, O. Long-term caffeine treatment of Alzheimer mouse models ameliorates behavioural deficits and neuron loss and promotes cellular and molecular markers of neurogenesis. *Cell. Mol. Life Sci.* **2022**, *79*, 55. [CrossRef]
24. Cao, C.; Cirrito, J.R.; Lin, X.; Wang, L.; Verges, D.K.; Dickson, A.; Mamcarz, M.; Zhang, C.; Mori, T.; Arendash, G.W. Caffeine suppresses amyloid-β levels in plasma and brain of Alzheimer's disease transgenic mice. *J. Alzheimer's Dis.* **2009**, *17*, 681–697. [CrossRef] [PubMed]
25. Arendash, G.W.; Cao, C. Caffeine and coffee as therapeutics against Alzheimer's disease. *J. Alzheimer's Dis.* **2010**, *20*, S117–S126. [CrossRef] [PubMed]
26. Brusco, L.I. Cognitive Decline and Treatment of Alzheimer's Disease. In *Neuropsychiatric Disorders*; Springer: Berlin/Heidelberg, Germany, 2010; pp. 213–226.
27. Rani, A.; Sodhi, R.K.; Kaur, A. Protective effect of a calcium channel blocker "diltiazem" on aluminum chloride-induced dementia in mice. *Naunyn-Schmiedeberg's Arch. Pharmacol.* **2015**, *388*, 1151–1161. [CrossRef] [PubMed]
28. Lukiw, W.J.; Cui, J.G.; Li, Y.; Bhattacharjee, P.S.; Corkern, M.; Clement, C.; Kammerman, E.M.; Ball, M.; Zhao, Y.; Hill, J. Acyclovir and Aβ42 peptide attenuates HSV-1-induced miRNA-146a levels in human brain cells. *Neuroreport* **2010**, *21*, 922. [CrossRef]
29. Hui, Z.; Zhijun, Y.; Yushan, Y.; Liping, C.; Yiying, Z.; Difan, Z.; Chunglit, C.T.; Wei, C. The combination of acyclovir and dexamethasone protects against Alzheimer's disease-related cognitive impairments in mice. *Psychopharmacology* **2020**, *237*, 1851–1860. [CrossRef]
30. Pyles, R.B. The association of herpes simplex virus and Alzheimer's disease: A potential synthesis of genetic and environmental factors. *Herpes* **2001**, *8*, 64–68.
31. Ren, J.; Hu, H.; Wang, S.; He, Y.; Ji, Y.; Chen, Y.; Wang, K.; Zhang, H.; Zhao, Y.; Dai, F. Prevent Drug Leakage via the Boronic Acid Glucose-Insensitive Micelle for Alzheimer's Disease Combination Treatment. *ACS Appl. Mater. Interfaces* **2022**, *14*, 20. [CrossRef]
32. Maiti, P.; Manna, J.; Burch, Z.N.; Flaherty, D.B.; Larkin, J.D.; Dunbar, G.L. Ameliorative Properties of Boronic Compounds in In Vitro and In Vivo Models of Alzheimer's Disease. *Int. J. Mol. Sci.* **2020**, *21*, 6664. [CrossRef]
33. Penland, J.G. The importance of boron nutrition for brain and psychological function. *Biol. Trace Elem. Res.* **1998**, *66*, 299–317. [CrossRef]
34. Lu, C.-J.; Hu, J.; Wang, Z.; Xie, S.; Pan, T.; Huang, L.; Li, X. Discovery of boron-containing compounds as Aβ aggregation inhibitors and antioxidants for the treatment of Alzheimer's disease. *MedChemComm* **2018**, *9*, 1862–1870. [CrossRef]
35. *CrysAlis PRO*; Agilent Technologies, UK Ltd.: Yarnton, UK, 2011.

36. Sheldrick, G. A short history of SHELX. *Acta Crystallogr. Sect. A* **2008**, *64*, 112–122. [CrossRef] [PubMed]
37. Sheldrick, G.M. SHELXT–Integrated space-group and crystal-structure determination. *Acta Crystallogr. Sect. A Found. Adv.* **2015**, *71*, 3–8. [CrossRef] [PubMed]
38. Dolomanov, O.V.; Bourhis, L.J.; Gildea, R.J.; Howard, J.A.; Puschmann, H. OLEX2: A complete structure solution, refinement and analysis program. *J. Appl. Crystallogr.* **2009**, *42*, 339–341. [CrossRef]
39. Faruggia, L. *ORTEP-3 V2. 02 for Windows*; University of Glasgow: Glasgow, UK, 2008.
40. Groom, C.R.; Bruno, I.J.; Lightfoot, M.P.; Ward, S.C. The Cambridge Structural Database. *Acta Crystallogr. Sect. B* **2016**, *72*, 171–179. [CrossRef]
41. Hernandez-Paredes, J.; Olvera-Tapia, A.L.; Arenas-Garcia, J.I.; Hopfl, H.; Morales-Rojas, H.; Herrera-Ruiz, D.; Gonzaga-Morales, A.I.; Rodriguez-Fragoso, L. On molecular complexes derived from amino acids and nicotinamides in combination with boronic acids. *Crystengcomm* **2015**, *17*, 5166–5186. [CrossRef]
42. Bhuvanesh, N.S.P.; Reibenspies, J.H. 4-Bromophenylboronic acid ethanol 0.04-solvate. *Acta Crystallogr. Sect. E* **2005**, *61*, o362–o364. [CrossRef]
43. TalwelkarShimpi, M.; Öberg, S.; Giri, L.; Pedireddi, V.R. Experimental and theoretical studies of molecular complexes of theophylline with some phenylboronic acids. *RSC Adv.* **2016**, *6*, 43060–43068. [CrossRef]
44. Chai, Z.; Wang, C.; Wang, J.; Liu, F.; Xie, Y.; Zhang, Y.-Z.; Li, J.-R.; Li, Q.; Li, Z. Abnormal room temperature phosphorescence of purely organic boron-containing compounds: The relationship between the emissive behaviorand the molecular packing, and the potential related applications. *Chem. Sci.* **2017**, *8*, 8336–8344. [CrossRef]
45. SeethaLekshmi, S.; Varughese, S.; Giri, L.; Pedireddi, V.R. Molecular Complexes of 4-Halophenylboronic Acids: A Systematic Exploration of Isostructurality and Structural Landscape. *Cryst. Growth Des.* **2014**, *14*, 4143–4154. [CrossRef]
46. Capillas, C.; Perez-Mato, J.M.; Aroyo, M.I. Maximal symmetry transition paths for reconstructive phase transitions. *J. Phys. Condens. Matter* **2007**, *19*, 275203. [CrossRef]
47. Bergerhoff, G.; Berndt, M.; Brandenburg, K.; Degen, T. Concerning inorganic crystal structure types. *Acta Crystallogr. Sect. B* **1999**, *55*, 147–156. [CrossRef] [PubMed]
48. de la Flor, G.; Orobengoa, D.; Tasci, E.; Perez-Mato, J.M.; Aroyo, M.I. Comparison of structures applying the tools available at the Bilbao Crystallographic Server. *J. Appl. Crystallogr.* **2016**, *49*, 653–664. [CrossRef]
49. Hernández-Negrete, O.; Sotelo-Mundo, R.R.; Esparza-Ponce, H.E.; Encinas-Romero, M.A.; Hernández-Paredes, J. New hydrate cocrystal of l-proline with 4-acetylphenylboronic acid obtained via mechanochemistry and solvent evaporation: An experimental and theoretical study. *J. Solid State Chem.* **2022**, *313*, 123282. [CrossRef]
50. Rodríguez-Cuamatzi, P.; Arillo-Flores, O.I.; Bernal-Uruchurtu, M.I.; Höpfl, H. Theoretical and experimental evaluation of homo- and heterodimeric hydrogen-bonded motifs containing boronic acids, carboxylic acids, and carboxylate anions: Application for the generation of highly stable hydrogen-bonded supramolecular systems. *Cryst. Growth Des.* **2005**, *5*, 167–175. [CrossRef]
51. Cartwright, A.C. *The British Pharmacopoeia, 1864 to 2014: Medicines, International Standards, and the State*; Ashgate: Surrey, UK; Burlington, VT, USA, 2015; p. 17.
52. Ramana, C.V.; Goriya, Y.; Durugkar, K.A.; Chatterjee, S.; Krishnaswamy, S.; Gonnade, R.G. Evaluation of viability of halogen[three dots, centered]O2N interactions: Insight from crystal packing in a series of isomeric halo and nitro substituted triaryl compounds with modular positioning of halogen and NO_2 groups. *Crystengcomm* **2013**, *15*, 5283–5300. [CrossRef]
53. Cavallo, G.; Metrangolo, P.; Milani, R.; Pilati, T.; Priimagi, A.; Resnati, G.; Terraneo, G. The Halogen Bond. *Chem. Rev.* **2016**, *116*, 2478–2601. [CrossRef]